

1 Multi-‘Omic Integration via Similarity Network Fusion

2 to Detect Molecular Subtypes of Aging

3 Mu Yang^{1,2}, Stuart Matan-Lithwick PhD², Yanling Wang MD PhD³, Philip L De Jager MD PhD⁴,
4 David A Bennett MD³, Daniel Felsky PhD^{1,2,4,6*}

5

6 1) Dalla Lana School of Public Health, University of Toronto, 155 College St Room 500, Toronto,
7 ON M5T 3M7, CA

8 2) The Krembil Centre for Neuroinformatics, Centre for Addiction and Mental Health, 12th Floor,
9 250 College Street, Toronto, ON, M5T 1R8, CA

10 3) Rush Alzheimer’s Disease Center, Rush University, 1750 W Harrison St, Chicago, IL 60612,
11 USA

12 4) The Center for Translational and Computational Neuroimmunology, Columbia University
13 Medical Center, 710 W 168th St, New York, NY 10033, USA

14 5) Department of Psychiatry, University of Toronto, 250 College Street, 8th floor, Toronto, ON,
15 M5T 1R8, CA

16 6) Institute of Medical Science, University of Toronto, 1 King’s College Circle, Medical Sciences
17 Building, Room 2374, Toronto, ON, M5S 1A8, CA

18

19 *Corresponding author

20 Daniel Felsky PhD

21 Independent Scientist, Krembil Centre for Neuroinformatics, Centre for Addiction and Mental Health

22 Assistant Professor, Department of Psychiatry and Dalla Lana School of Public Health, University of Toronto

23 12th Floor, 250 College Street, Toronto ON, M5T 1R8, Canada

24 Daniel.felsky@camh.ca; dfelsky@gmail.com

25 www.felskylab.com

26 (416) 535 8501 x33587

27 Abstract

28 **Background:** Molecular subtyping of brain tissue provides insights into the heterogeneity of
29 common neurodegenerative conditions, such as Alzheimer's disease (AD). However, existing
30 subtyping studies have mostly focused on single data modalities and only those individuals with
31 severe cognitive impairment. To address these gaps, we applied Similarity Network Fusion (SNF),
32 a method capable of integrating multiple high-dimensional multi-'omic data modalities
33 simultaneously, to an elderly sample spanning the full spectrum of cognitive aging trajectories.

34 **Methods:** We analyzed human frontal cortex brain samples characterized by five 'omic modalities:
35 bulk RNA sequencing (18,629 genes), DNA methylation (53,932 cpg sites), histone H3K9
36 acetylation (26,384 peaks), proteomics (7,737 proteins), and metabolomics (654 metabolites).
37 SNF followed by spectral clustering was used for subtype detection, and subtype numbers were
38 determined by eigen-gap and rotation cost statistics. Normalized Mutual Information (NMI)
39 determined the relative contribution of each modality to the fused network. Subtypes were
40 characterized by associations with 13 age-related neuropathologies and cognitive decline.

41 **Results:** Fusion of all five data modalities ($n=111$) yielded two subtypes ($n_{s1}=53$, $n_{s2}=58$) which
42 were nominally associated with diffuse amyloid plaques; however, this effect was not significant
43 after correction for multiple testing. Histone acetylation (NMI=0.38), DNA methylation (NMI=0.18)
44 and RNA abundance (NMI=0.15) contributed most strongly to this network. Secondary analysis
45 integrating only these three modalities in a larger subsample ($n=513$) indicated support for both
46 3- and 5-subtype solutions, which had significant overlap, but showed varying degrees of internal
47 stability and external validity. One subtype showed marked cognitive decline, which remained
48 significant even after correcting for tests across both 3- and 5-subtype solutions ($p_{\text{Bonf}}=5.9 \times 10^{-3}$).
49 Comparison to single-modality subtypes demonstrated that the three-modal subtypes were able

50 to uniquely capture cognitive variability. Comprehensive sensitivity analyses explored influences
51 of sample size and cluster number parameters.

52 **Conclusion:** We identified highly integrative molecular subtypes of aging derived from multiple
53 high dimensional, multi-'omic data modalities simultaneously. Fusing RNA abundance, DNA
54 methylation, and H3K9 acetylation measures generated subtypes that were associated with
55 cognitive decline. This work highlights the potential value and challenges of multi-'omic integration
56 in unsupervised subtyping of postmortem brain.

57 **Keywords:** multi-'omic Integration, molecular subtyping, cognitive aging, Alzheimer's disease,
58 postmortem brain, clustering analysis

59

60 **Introduction**

61 Aging is often accompanied by progressive cognitive decline. The severity of this decline ranges
62 from normal age-related changes to clinically important mild cognitive impairment (MCI) and
63 ultimately dementia [1,2]. Alzheimer's disease (AD) is the most common cause of late-life
64 dementia, which is typically characterized by impairments in memory and loss of daily functioning
65 [2]. This poses a major public health concern, as by 2050, the estimated number of individuals
66 diagnosed with dementia globally is expected to reach 152.8 million [3]. As a neuropathological
67 process, AD is defined by the abnormal accumulation of neurofibrillary tangles
68 (hyperphosphorylated tau protein), the formation of extracellular dense core plaque deposits
69 (beta-amyloid), and chronic neuroinflammation in the brain [4]. However, there is great inter-
70 individual heterogeneity in these pathological hallmarks, and the relationship between
71 neuropathology and cognitive impairment is not deterministic [5]. As such, there likely remain

72 unobserved molecular signatures of age-related cognitive decline that could help explain the
73 heterogeneity observed within populations and shed light on mechanisms of illness.

74 Molecular subtyping most often refers to classifying individuals within a population into subgroups
75 using molecular data types and unsupervised clustering methods [6,7]. The approach has seen
76 success in fields with abundant and readily assayed tissue samples from diseased populations,
77 such as in oncology, where biopsied tumors yield molecular information leading to precision
78 interventions [7]. Similarly, the heterogeneity of cognitive aging may be partly explained by using
79 high-dimensional molecular measures from postmortem brain tissue of elderly donors to group
80 similar individuals. For example, molecular subtypes of AD derived from RNA sequencing
81 (RNAseq) data have been associated with AD-relevant pathologies [8–11], including amyloid and
82 tau neuropathological burden, and *APOE* genotype [8,9]. Subtypes derived from common genetic
83 variation, specifically single nucleotide polymorphisms, identified multiple AD-related molecular
84 mechanisms [12]. A major limitation of most existing subtyping studies in this field is that they rely
85 on information from single data modalities, e.g. gene expression data, which greatly constrains
86 the information used to parse biological systems and pathological processes [13,14].

87 Importantly, it has been shown that several multi-‘omic data types, including histone acetylation
88 [15], metabolomics [16–20] and proteomics [21], are not only associated with AD
89 neuropathologies, but also contributed information to associations that is missed with RNAseq
90 alone [8,21]. As such, integrating data modalities into subtyping pipelines has been an active area
91 of research [22,23], and large-scale cohort studies of aging that include brain donation and multi-
92 ‘omic characterization, such as those from the Accelerating Medicines Partnership for Alzheimer’s
93 Disease (AMP-AD) consortium, now offer opportunities for developing highly integrative models
94 of cognitive decline [24]. Methods development in high-dimensional feature integration have also
95 facilitated these analyses [25,26], though not yet in pathological aging or AD. Similarity network

96 fusion (SNF) is a network-based method specifically developed to integrate several multi-'omic
97 data modalities simultaneously [27].

98 Here we performed a highly integrative analysis on up to five postmortem multi-'omic data
99 modalities simultaneously, measured in the same individuals, to identify molecular subtypes of
100 aging using the SNF method. We then characterized these subtypes by associating subtype
101 membership with 13 age-related neuropathologies, antemortem cognitive performance, and rates
102 of longitudinal cognitive decline. The most important features contributing to the fully fused
103 similarity network were identified and subsequent analyses focused on the most informative data
104 modalities. Lastly, we performed comprehensive sensitivity testing to explore the effects of
105 parameter selection in unsupervised multi-'omic subtyping, which are often chosen arbitrarily.

106

107 **Methods**

108 **Study participants**

109 Data were analyzed from two longitudinal cohort studies of aging and dementia: the Religious
110 Orders Study and Rush Memory and Aging Project (ROS/MAP), with more than 3,500
111 predominantly white elderly (mean = 78.44, sd = 7.79) participants of mostly European descent
112 without known dementia at the time of enrollment [28]. Participants in ROS (1994-present) are
113 older Catholic priests, nuns, and brothers across the United States, whereas MAP (1997-ongoing)
114 recruits primarily from retirement communities and via social service agencies and Church groups
115 throughout northeastern Illinois [28,29]. Combined data analysis for these two cohorts are
116 enabled by harmonized protocols for participant recruitment, clinical assessment, and

117 neuropathological examination at autopsy (autopsy rate exceeding 86%) with a large common
118 core of identical item level data. A Rush University Medical Center Institutional Review Board
119 approved each study. All participants signed an Anatomic Gift Act as well as informed and
120 repository consents. Annual visits include tests of cognition function and a broad range of other
121 demographic, social, lifestyle, and clinical assessments with an averaged follow-up rate of 97%
122 [29]. Further details about the ROS and MAP cohorts can be found in previous publications [30]
123 and through the Rush Alzheimer's Disease Center Research Resource Sharing Hub, where
124 participant-level clinical and demographic data are available via restricted access
125 (<https://www.radc.rush.edu/home.htm>).

126 ***Multi-‘omic data used for subtyping***

127 We used five multi-‘omic data modalities to identify molecular subtypes: bulk RNAseq (18,629
128 genes, $n_{RNAseq}=1,092$), DNA methylation (53,932 cpg sites, $n_{DNA}=740$), histone H3K9 acetylation
129 (26,384 peaks, $n_{histone}=669$), metabolomics (654 metabolites, $n_{metabolomics}=514$), and tandem mass
130 tag (TMT) proteomics (7,737 proteins, $n_{proteomics}=368$). All data types were acquired from the same
131 brain region postmortem: dorsolateral prefrontal cortex (DLPFC). All ‘omic datasets used in our
132 analyses were generated by members of the Accelerating Medicines Partnership - Alzheimer’s
133 disease (AMP-AD) consortium and are available via restricted access through the AMP-AD
134 knowledge portal, on Synapse (<https://adknowledgeportal.synapse.org/>). Further details can be
135 found in Acknowledgements.

136 **RNA sequencing (RNAseq)**

137 Full details on gene-level expression data from bulk DLPFC tissue have been published [31].
138 Approximately 100 mg of DLPFC tissue were dissected from autopsied brains. Samples were
139 processed in batches of 12–24 samples for RNA extraction using the Qiagen MiRNeasy Mini (cat

140 no. 217004) protocol, including the optional DNase digestion step. RNA Samples were submitted
141 to the Broad Institute's Genomics Platform for transcriptome library construction following
142 sequencing in three batches using the Illumina HiSeq (batch #1: 50M 101bp paired end reads)
143 and NovaSeq6000 (batch #2: 30M 100bp paired end; batch#3: 40-50M 150bp paired end 121
144 reads) [32]. A cut-off point of 5 for RNA Integrity Number (RIN) score was used for constructing
145 the cDNA library [33]. The average sequencing depth was 50 million paired reads per sample. To
146 achieve higher quality of alignment results, a paralleled and automatic RNAseq pipeline was
147 implemented based on several Picard metrics (<http://broadinstitute.github.io/picard/>). 18,629
148 features - full-length gene transcripts - from 1,092 samples remained after data preprocessing
149 and quality control (QC).

150 DNA methylation

151 Tissues were dissected similar to gene-expression data, full details on DNA methylation data
152 have been published [33]. DNA was extracted by the Qiagen QIAamp mini protocol (Part number
153 51306). Probes with p-value >0.01 were removed at probe level QC if predicted to cross-hybridize
154 with sex chromosomes and having overlaps with known SNP with MAF ≥ 0.01 (± 10 bp) based on
155 the 1000 Genomes database. Subject level QC methods including principal component analysis
156 and bisulfite conversion efficiency. β -values reported by the Illumina platform were used as the
157 measurement of methylation level for each CpG probe tagged on the chip; where missing values
158 were imputed by the k-nearest neighbor algorithm (k=100). The primary data analysis was
159 adjusted by age, sex, and experiment batch [33]. Due to the large number of features present for
160 this data type, and to limit computational time, we only included the top 53,932 methylation peaks
161 showing the greatest variability (**Supplementary Figure 1A**). To verify that this selection process
162 did not impact our subtyping efforts, we performed sensitivity analysis for 5-modal integration

163 using all CpG sites - resulting subtype memberships were nearly identical (**Supplementary**
164 **Figure 1B**).

165 Histone H3K9 acetylation

166 For the acetylation of the ninth lysine of histone 3 (H3K9ac), which is a marker of open chromatin,
167 the Millipore anti-H3K9ac mAb (catalog #06-942, lot: 31636) was identified as a robust
168 monoclonal antibody for the chromatin immunoprecipitation experiment. Similar to RNAseq and
169 DNA methylation, 50 milligrams of gray matter was dissected on ice from biopsies of the DLPFC
170 of each participant of ROS/MAP. Chromatin labeled with the H3K9ac mark and bound to the
171 antibody was purified with protein A Sepharose beads [15]. To quantify histone acetylation, single-
172 end reads were aligned to the GRCh37 reference genome by the BWA algorithm after sequencing.
173 Picard tools were used to flag duplicate reads. A combination of five ChIP-seq quality measures
174 were employed to detect low quality samples: samples that did not reach (i) $\geq 15 \times 10^6$ uniquely
175 mapped unique reads, (ii) non-redundant fraction ≥ 0.3 , (iii) cross correlation ≥ 0.03 , (iv) fraction of
176 reads in peaks ≥ 0.05 and (v) ≥ 6000 peaks were removed [15]. Samples passing QC were used to
177 define a common set of peaks termed H3K9ac domains. H3K9ac domains of less than 100bp
178 width were removed resulting in a total of 26,384 H3K9ac domains with a median width of
179 2,829 bp available for 669 subjects. Full details on H3K9ac data can be found on Synapse
180 (<https://www.synapse.org/#!Synapse:syn4896408>).

181 Metabolomics

182 Metabolomics data were generated by the Alzheimer's Disease Metabolomics Consortium
183 (ADMC; ADMC members list <https://sites.duke.edu/adnimetab/team/>), led by Dr. Rima Kaddurah-
184 Daouk [18–20]. Metabolomic profiling of postmortem brain was conducted at Metabolon (Durham,
185 NC) with the Discovery HD4 platform consisting of four independent ultra-high-performance liquid

186 chromatography–tandem mass spectrometry (UPLC–MS/MS) instruments [16,17]. For the
187 purpose of QC and better understanding of the underlying biological mechanisms, missing rates
188 less than 20% on known metabolites and 40% on individuals were imposed. As SNF cannot
189 handle missing data, random forest imputation [34] was then applied, resulting in 654 metabolites
190 and 514 individuals. Full details on metabolomic assays and data processing can be found here
191 (<https://www.synapse.org/#ISynapse:syn26007830>). The full metabolomics dataset and
192 metadata can be accessed via the AMP-AD Knowledge Portal.

193 Proteomics

194 Prior to TMT labeling, samples were randomized by co-variates (age, sex, postmortem interval
195 (PMI), diagnosis, etc.), into 50 total batches (8 samples per batch) [35]. Peptides from each
196 individual (n=400) and the GIS pooled standard (n=100) were labeled using the TMT 10-plex kit
197 (ThermoFisher 90406). Peptide eluents were separated on a self-packed C18 (1.9 µm, Dr. Maisch)
198 fused silica column (25 cm × 75 µM internal diameter) by a Dionex UltiMate 3000 RSLCnano liquid
199 chromatography system (Thermo Fisher Scientific) [35,36]. Peptides were monitored on an
200 Orbitrap Fusion mass spectrometer (Thermo Fisher Scientific). The mass spectrometer was set
201 to acquire data in positive ion mode using data-dependent acquisition. Dynamic exclusion was
202 set to exclude previously sequenced peaks for 20 s within a 10-ppm isolation window [35,36]. In
203 this study we only include peptides and participants with a missing rate less than 20% followed
204 by random forest imputation [37], resulting in 7,737 proteins and 386 individuals. Full details on
205 proteomics data acquisition and processing can be found on synapse
206 (<https://www.synapse.org/#ISynapse:syn17015098>).

207 ***Uniform multi-‘omic feature post-processing***

208 Due to differences in data feature preprocessing among the five selected ‘omic data modalities,
209 we performed additional post-processing QC to determine whether technical and demographic
210 covariates may be influencing global patterns of variability for each modality. To achieve this, we
211 tested associations between age of death, sex, PMI, and study cohort (ROS vs. MAP) with each
212 of the top 20 components from PCA for each ‘omic modality separately, as in previous ‘omic work
213 in this cohort [31]. The proportion of variance explained by each PC from each of the five data
214 modalities, and the corresponding associations of each PC with potential covariates, are shown
215 in **Supplementary Figures 2-6**. Based on this assessment, we determined that four out of five
216 data modalities showed significant associations of all four covariates within the first 10 principal
217 components (RNAseq data had been post-processed already and residualized for each of these
218 covariates in addition to modality-specific confounders). We therefore proceeded by residualizing
219 all features from each modality according to a linear model including all four covariates. This
220 conservative approach ensured that contributions of each modality to latent subgroups were not
221 unbalanced by different representations of covariate-specific effects. We also performed
222 iterations of the analysis without correction, finding very similar but not identical subgroup
223 memberships for 5-modal integration (**Supplementary Figure 7**).

224 ***Neuropathological assessment***

225 All selected postmortem neuropathological variables analyzed in this study have been previously
226 published in detail [29,38]. In addition to the outcome of NIA-Reagan neuropathological diagnosis
227 of Alzheimer’s disease [5,39], we examined 13 other individual pathologies: brainwide amyloid-
228 beta, diffuse and neuritic plaque counts, paired helical filament tau, neurofibrillary tangle count,
229 TDP-43 proteinopathy stage (4 levels), large vessel cerebral atherosclerosis rating (4 levels),
230 arteriolosclerosis, semiquantitative summary of cerebral amyloid angiopathy pathology (CAA; 4

231 levels), pathologic stage of Lewy body disease (4 stages), gross chronic cerebral infarcts (coded
232 as binary; presence/absence of infarcts), and cerebral microinfarcts (coded as binary;
233 presence/absence of infarcts).

234 ***Cognitive performance and residual cognition (resilience)***

235 Scores from five cognitive domains (episodic memory, semantic memory, working memory,
236 perceptual speed and perceptual orientation) were recorded at last study visit and summarized
237 by z-scoring for a composite measure of global cognition, as described [40]. In our study, we
238 defined the last available global cognitive measure as cognitive performance proximal to death.
239 Cognitive slopes were also derived from the same set of z-scores over time to measure the
240 longitudinal aspect of cognitive decline [41]. To assess the resilience component of an individual's
241 cognitive capacity, we used the residual cognition approach [42,43]. Residual cognition was
242 defined as the residuals of a linear model of global cognitive performance at last visit regressed
243 on observed neuropathologies (beta-amyloid, neurofibrillary tangles, neuritic plaques, diffuse
244 plaques, Lewy bodies, macroscopic infarcts, microscopic infarcts, atherosclerosis,
245 arteriolosclerosis, TDP-43 and CAA).

246 ***Statistical Analysis***

247 ***Subtype identification with Similarity Network Fusion (SNF)***

248 The Similarity Network Fusion (SNF) method was used to integrate multi-'omic data modalities
249 [27]. SNF first constructs sample-by-sample similarity matrices for each data modality separately
250 and then iteratively updates and integrates these matrices via nonlinear combination until
251 convergence is reached, generating a fused similarity network [44]. SNF does not require any
252 prior feature selection, but fully imputed (non-missing) data is required. According to best

253 practices [35,37], random forest imputation was applied on both metabolomics and proteomics
254 data to impute missing values. The 'SNFtool' R package (v2.2.0) was used for the network fusion
255 pipeline, with recommended parameters $K=40$, $\alpha=0.5$, and $T=50$ (where K is the number of
256 neighbors used to construct the similarity matrices; α is a hyper-parameter used in the scaling
257 of edge weights; T is the total number of algorithmic iterations). Spectral clustering, an
258 unsupervised soft clustering method rooted in graph theory [27,45], is the default clustering
259 method for 'SNFtool'; it was applied to the full fused affinity matrix to cluster study participants
260 into subtypes. Optimal cluster numbers were identified (2 to 8 clusters) by the rotation cost [46]
261 and eigen-gap [45] methods. Data modalities contributing the most information to fused similarity
262 matrices were computed by Normalized Mutual Information (NMI). NMI is a measure of relevance
263 and redundancy among features [47], which helps to identify the data types that contribute most
264 strongly to the fused network estimated by SNF [27].

265 Assessment of internal subtype validity

266 Due to the high dimensionality and heterogeneity of multi-'omic data, assessments of cluster
267 validity are critical to tackling potential biases of clustering algorithms toward particular cluster
268 properties and to evaluate the probability that clusters do in fact exist [48,49]. Upon subtype
269 identification, we conducted internal cluster stability analysis using the R package 'clValid', which
270 measures cluster validity and stability through several metrics derived from resampling and cross-
271 validation. Metrics included in our studies are the average proportion of non-overlap (APN) and
272 the average distance between means (ADM), which work especially well if the data are highly
273 correlated, which is often the case in high-throughput genomic data [49–51]. For resampling, we
274 pulled 80% of participants for a total of 300 random draws, in accordance with previously
275 published work using the SNF pipeline [52] as well as other AD molecular subtyping efforts [8].
276 The adjusted Rand index (ARI) was used to measure the agreement between subtype

277 membership solutions (ranging from 0 to 1, where ARI = 1 indicating perfect agreement) [53]. Chi-
278 square statistics were also used to compare the independence between different subtyping
279 solutions [54].

280 Identifying top individual features defining molecular subtypes

281 In order to identify molecular features that differed most between subtypes after spectral
282 clustering, we performed one-way ANOVA tests between each normalized feature from each
283 multi-‘omic data modality and subtype groupings. P-values from F-tests were used as the
284 measure of significance to rank features from each modality. Gene annotations for DNA
285 methylation data were mapped using the UCSC genome browser [55], and histone acetylation
286 peaks were annotated by Klein et al. [15].

287 Association of subtypes with neuropathology, cognition, and residual 288 cognition

289 For each clustering solution, subtype membership was initially characterized by associations with
290 13 neuropathologies and three cognitive measures described above using linear or logistic
291 regression. Subtype membership for each participant was represented with dummy variables for
292 inclusion in each model ($n_{\text{subtypes}}-1$). For models of neuropathology, co-variates included age at
293 death, biological sex, educational attainment (years), PMI, study cohort, and *APOE ε4* status.

294 (A) Neuropathologies ~ Subtype + Age of death + Sex + Education + PMI + Study + *APOE*
295 ε4

296 When fitting regression models for cognitive outcomes, the model (B) was also adjusted for the
297 measurement latency, which is equal to the time difference (in years) between the last study visit
298 where cognitive performance was assessed and age of death.

299 (B) Cognitive Measurements ~ Subtype + Latency + Age of death + Sex + Education + PMI +
300 Study + *APOE ε4*

301 Omnibus F-tests of the hypothesis of equal outcome means (or probabilities for logistic models)
302 across all subtypes were used to test the significance of subtype membership effects. *P*-values
303 were Bonferroni adjusted for 16 tested outcomes, except where otherwise indicated. For subtypes
304 with significant effects on global cognition (either at last visit or longitudinal slope), secondary
305 analyses were performed (according to model B) for each subdomain of cognition separately.

306 **Sensitivity analyses for external validity across data modalities, sample sizes,**
307 **and cluster numbers**

308 To better understand the added value of data integration in the context of molecular subtyping,
309 we performed a set of sensitivity analyses to measure differences in neuropathological and
310 cognitive relevance (external validity) of subtypes derived from different combinations of multi-
311 'omic data modalities. Given that each iteration of these integrative analyses was limited to the
312 sample size in which all data types were non-missing, we also assessed the effects of performing
313 clustering in artificially limited sample subsets (i.e., where included non-missing data modalities
314 permit a larger sample size). To achieve this, we defined a full search space of analytical pipeline
315 configuration and parameter combinations for exhaustive modeling: 1) data modalities included
316 (d ; 31 possible combinations), 2) sample size (n ; ranging from 111 to 1,092 participants, including
317 31 possible sample sizes each corresponding to a different data modality combination), and 3)
318 cluster number (c ; ranging from 2-5, the extremes of values observed in our subtyping analyses).
319 This resulted in a total of 844 unique combinations of d , n , and c . To evaluate external validity,
320 we performed omnibus tests of the association of subtype membership for each analytical
321 iteration with the set of neuropathologies and cognitive measures, as previously. To provide some
322 generalized insight into the effects of manipulating design parameters on our association

323 strengths, second-level analyses were performed by relating each pipeline parameter to observed
324 omnibus model significance for each neuropathology and cognitive outcome (j). For these
325 analyses, the effects of c (and cf , the same parameter but treated as a categorical variable), n ,
326 and a new parameter, m , representing the number of data modalities being fused, were tested
327 independently, according to the following formulae:

328 $(C) -\log(p_j) \sim m, -\log(p_j) \sim n, -\log(p_j) \sim c$

329

330 **Results**

331 We analyzed data from a total of 1,314 unique participants from the Religious Orders Study and
332 Memory and Aging Project (ROS/MAP) with at least one available multi-'omic data modality and
333 non-missing clinical and neuropathological data. Sample demographics are summarized in **Table**
334 **1**. The number of participants with different degrees of overlapping multi-'omic characteristics
335 ranged from $n=111$ (all five data types) to 1,092 (RNAseq only); all overlaps are shown in **Figure**
336 **1A**.

337 ***Fully integrated five-modal network identifies two molecular subtypes***
338 ***nominally associated with neuritic plaque burden***

339 First, we aimed to determine whether molecular subtypes derived from all five multi-'omic data
340 modalities were informative of postmortem neuropathology and antemortem cognitive decline.
341 SNF yielded an optimal solution of two molecular subtypes (**Figure 1B**) in 111 individuals with all
342 five 'omic modalities ($n_{S1}=53, n_{S2}=58$). Both the rotation cost and eigen-gap methods elected two
343 as the optimal number of clusters. These subtypes were weakly associated with neuritic ($p_{raw}=$

344 0.09) and diffuse plaque counts ($p_{\text{raw}}=0.03$), though these associations did not survive correction
345 for multiple testing. In addition, no significant associations were observed for cognitive
346 performance at last visit, rate of cognitive decline, or residual cognition (**Figure 1C**).

347 Despite the lack of significant associations of molecular subtypes with pathology and cognition,
348 the fully fused network demonstrated substantial internal stability (APN=8.7%, ADM=0.02;
349 **Supplementary Figure 8**). We therefore proceeded to identify the data modalities contributing
350 most to the fused network by normalized mutual information (NMI) (**Supplementary Table 1**).
351 We found that histone acetylation (NMI=0.38), DNA methylation (NMI=0.18) and RNAseq
352 (NMI=0.15) were the top contributors to the fused network (to a substantially greater degree than
353 proteomic (NMI=0.04) and metabolomic modalities (NMI=0.05)). The top 10 individual features
354 contributing to the fused network from the top contributors are summarized in **Supplementary**
355 **Table 2**. Based on the importance of the top three data modalities, secondary analysis was
356 conducted integrating only histone acetylation, DNA methylation, and RNAseq, which permitted
357 subtyping of a much larger sample size with non-missing overlapping data (n=513).

358 ***Subtypes derived from three-modal integration are associated with***
359 ***cognitive performance proximal to death and longitudinal cognitive***
360 ***decline***

361 In secondary analyses with three data modalities, the eigen-gap method elected three molecular
362 subtypes as the optimal clustering solution, while rotation cost elected five. We therefore
363 evaluated both solutions by comparing membership overlap, differences in internal validity metrics,
364 and associations with neuropathology and cognition. A strong overlap was identified between
365 subtype memberships in the 3- and 5-subtype solutions (chi-square $p=2.2\times 10^{-16}$, ARI=0.76;
366 **Figure 2A, D**), whereby the large subtype 3 (n=377) from the 3-subtype solution contained 81.2%

367 of the participants assigned to subtypes 3, 4, and 5 from the 5-subtype solution. Internal cluster
368 stability was compared between 3-subtype and 5-subtype solutions (**Figure 2B, C**); both APN
369 and ADM measures were better for the 3-subtype solution (APN=9.6%, ADM=0.01), though the
370 5-subtype solution also demonstrated cluster stability well above random chance (APN=23.1%,
371 ADM=0.02) (**Figure 2E, F**).

372 In tests of external validity, and tests of association with neuropathological and cognitive
373 measures, subtype membership was significantly associated with global cognition at last visit
374 ($p_{\text{Bonf}}=0.022$) and rate of cognitive decline ($p_{\text{Bonf}}=4.2 \times 10^{-4}$) for the 5-subtype solution after multiple
375 testing correction (**Figure 2G**). In contrast, the 3-subtype solution was preferred by internal cluster
376 stability metrics, and significant associations with neuropathology or cognition were not observed
377 (**Figure 2G**). We therefore probed further into the 5-subtype solution.

378 Cross-tabulation of three-modal and five-modal subtype memberships was carried out for only
379 the 111 individuals included in the full five-modal analysis above, finding substantial overlap (chi-
380 square $p=8.1 \times 10^{-9}$, ARI=0.60; **Figure 3A**). This demonstrated that the SNF procedure was
381 consistent across sample size in terms of defining core cluster memberships when the most
382 influential data types were combined.

383 In assessments of the mean differences in global cognition and the ratio of cognitive decline
384 across 5 subtypes identified, subtype 5 had the worst global cognitive performance at last visit
385 and the fastest rate of cognitive decline (**Figure 3B**). This difference was significant in post hoc
386 pairwise tests against all other subtypes, except for subtype 2 (**Figure 3C**). Subtype 4 exhibited
387 the best average cognitive performance and slowest decline (**Figure 3B, C**). Notably, the
388 association observed with cognitive decline ($p_{\text{Bonf}}=5.9 \times 10^{-3}$) was strong enough to survive
389 correction for multiple testing across combined 5-subtype and 3-subtype association test sets (32
390 tests) (**Figure 2G**). Given the significant association of subtypes with global cognition at last visit

391 and rate of global cognitive decline, we performed follow-up analysis on five cognitive subdomains.
392 For rate of cognitive decline, subtypes were most strongly associated with perceptual orientation
393 ($p_{\text{Bonf}}=8.0 \times 10^{-5}$), perceptual speed ($p_{\text{Bonf}}=0.004$), and semantic memory ($p_{\text{Bonf}}=0.007$)
394 (**Supplementary Figure 9A**). Specifically, the best and worst cognitive performance values were
395 observed on average in subtypes 4 and 5, respectively (**Supplementary Figure 9B-F**). A similar
396 pattern was also identified from cognition measured at last visit (**Supplementary Figure 9G-L**).

397 **Molecular features defining three-modal subtypes**

398 To describe the molecular signals most strongly associated with our observed subtypes, we first
399 identified the top features contributing to the fused network from each data modality by ANOVA
400 (**Supplementary Table 3**). The top 5 histone acetylation features exhibited the strongest within-
401 subtype homogeneity and between-subtype variability (consistent with the observation that
402 histone acetylation had the largest NMI of each modality **Supplementary Table 1**). The most
403 extreme values for acetylation were observed in subtypes 1 (lowest levels) and 2 (highest levels)
404 at peaks annotated to *ZNF219*, *TMEM153*, *LSM14A*, *PSMD11*, *CDK5R1*, *MYD1D*, *ALDH3A2*,
405 *APBB2*, and others (**Figure 3D**). Subtype 5, which was characterized by the fastest rate of
406 cognitive decline, had intermediate acetylation of these peaks (along with subtype 4, which are
407 largely represented by subtype 3 in the 3-subtype solution). For DNA methylation, CpG sites
408 showed differential methylation at sites annotated to *RB1*, *LPAR6*, and *RP11-83B20.10*, as well
409 as intergenic regions on chromosome 5 and 7, though no consistent pattern related to the
410 cognition-associated subtype 5 was observed (**Figure 3F**). In contrast, the top subtype-
411 associated RNAseq features revealed lower levels of *PCYOX1L* and *NECTIN1*, as well as higher
412 levels of *SLC5A3*, *PPP4R2*, and *PPP1CC* in subtype 5 specifically compared to all other subtypes
413 (**Figure 3E**).

414 **Comparison with single modality subtypes and sensitivity analysis**

415 Finally, we compared clinical and neuropathological associations of these three-modal subtypes
416 with those for subtypes derived from each of the modalities analyzed individually. We found that
417 these integrated subtypes had unique associations with cognitive performance and decline. For
418 example, subtypes derived from RNAseq alone ($n=1,092$) were significantly associated with
419 amyloid-beta ($p_{\text{Bonf}}=0.018$) and neuritic plaque burden ($p_{\text{Bonf}} = 2.3 \times 10^{-3}$), but not with global
420 cognition at last visit ($p_{\text{Bonf}}=0.28$) or rate of cognitive decline ($p_{\text{Bonf}}=1.0$). In fact, none of the
421 unimodal subtypes showed more significant associations than three-modal, 5-cluster subtypes on
422 global cognitive performance (**Figure 3G**).

423 In sensitivity analyses, substantial variability in external validity was observed across different
424 selections of sample size, data modalities, and cluster number. **Supplementary Figure 10**
425 illustrates the full set of results for selected amyloid and cognitive outcomes, which were the
426 outcomes demonstrating the most significant associations with subtype membership in our
427 analyses above (full summary statistics from these analyses are available in **Supplementary**
428 **Table 4**). **Supplementary Figure 11A** shows the meta-regression results for the influence of
429 sample size (n), number of data modalities (m), and cluster number (c) on statistical associations
430 with all 16 tested phenotypes. Generally, less significant associations were captured as more data
431 modalities were integrated and sample size decreased (see example of beta-amyloid in
432 **Supplementary Figure 11B**), though exceptions were noted, such as for Lewy bodies (where
433 additional modalities on average increased external validity; meta $p_{\text{raw}}=2.5 \times 10^{-7}$; **Supplementary**
434 **Figure 11C**). Comparatively, cluster number selection had less of an impact overall on external
435 validity.

436

437 **Discussion**

438 We used up to five 'omic data modalities acquired from the human postmortem prefrontal cortex
439 simultaneously to detect molecular subtypes of aging using a high-dimensional, unsupervised
440 approach. We identified several subtypes that were significantly associated with individuals' rates
441 of cognitive decline and levels of beta-amyloid neuropathology. In particular, molecular subtypes
442 derived from a three-modal integrated network combining gene expression (RNAseq), H3K9ac,
443 and DNA methylation peaks yielded subtypes of participants with significantly faster decline in
444 global cognition, specifically in domains of perceptual orientation, perceptual speed, and semantic
445 memory. To the best of our knowledge, associations between multi-'omic subtypes and cognitive
446 performance have not previously been identified, and most subtyping studies have focused only
447 on individuals with confirmed, late-stage AD [56]. Our findings also empirically quantify the relative
448 information provided by different 'omic modalities to participant similarity networks.

449 In fully integrated analyses, combining all five available modalities, we identified two molecular
450 subtypes which exhibited non-significant external validity with respect to neuropathology and
451 cognition. We did not explore this result much further for three reasons: 1) both internal cluster
452 validity metrics (eigen gap and rotation cost) elected the same 2-subtype solution, 2) the sample
453 size for full five-modal integration analysis was small (n=111), and 3) NMI calculations showed
454 substantial heterogeneity in the amount of information contained within each modality when
455 considering patient similarity networks in this sample subset. The small sample size was likely a
456 key limitation; this was confirmed by sensitivity analyses showing that even for single data
457 modalities, when the sample was restricted to the n=111 group, there were virtually no observed
458 associations with any cognitive or neuropathological measures.

459 By comparing both integrated molecular subtypes and unimodal subtypes from spectral clustering,
460 we found that subtypes from RNAseq alone were significantly associated with neurofibrillary
461 tangles and amyloid-beta. Such associations align with findings from previous subtyping work in
462 only individuals suffering from dementia [8], and demonstrate the reliability of the method we used
463 for subtyping. Our analysis also emphasizes the importance of integrating epigenetic data with
464 gene expression studies seeking to identify key molecular drivers of AD [57]. Variability in gene
465 expression alone cannot determine the current status of diseases [58,59]; even so, genetic and
466 epigenetic studies still tend to be conducted separately [57]. This study serves as evidence that
467 integrating multiple epigenetic data types with gene expression data can lead to the discovery of
468 novel molecular subtypes associated with cognition.

469 In describing the top molecular features that distinguish our subtypes from one another, we
470 identified epigenetic marks and RNA transcripts which map to genomic loci previously associated
471 with AD and cognitive aging. Of particular interest were those loci that differentiated cognition-
472 associated subtype 5 from all other subtypes. In this subtype, we found lower levels of
473 Prenylcysteine Oxidase 1 Like (*PCYOX1L*), a gene which has been previously associated with
474 AD [60–63], and has been identified as an AD target gene by the Agora platform
475 (<https://agora.adknowledgeportal.org/>) with strong evidence for RNA down-regulation across 8
476 brain regions and proteomic down-regulation across four regions. Nectin cell adhesion molecule
477 1 (*NECTIN1*) [64] was similarly downregulated in subtype 5, and also showed RNA and protein-
478 level dysregulation in the Agora database, confirming that the multi-modal SNF pipeline was
479 capable of extracting some known signals with neuropathological significance.

480 Among the top genes with higher average levels in subtype 5 were *SLC5A3* [65], *PPP4R2*, and
481 *PPP1CC*. *PPP4R2* and *PPP1CC* code for enzymes in the serine/threonine-protein phosphatase
482 family and are well-known contributors to canonical AD pathological cascades [66]. Interestingly,
483 *PPP4R2* has also been identified as a top hypomethylated gene of interest in a methylome-wide

484 association study of Parkinson's disease [67], an illness which is also often accompanied by
485 cognitive decline [68]. Other top contributors to the three-modal subtypes, such as *PSMD11* [69],
486 *APBB2* [70], and *TMEM253* [71] are also known to be involved in the development of AD
487 pathology. *TMEM253* is also linked with mild cognitive impairment (MCI) via predicted gene
488 expression based on genetic variation (TWAS) [71]. However, some top genes (e.g. *ZNF219*, a
489 Kruppel-like zinc finger gene, has been associated with a-synucleinopathy [72] and has binding
490 sites in the *MAPT* gene [73]). In contrast, these genes have not yet been associated with AD or
491 cognitive aging, and our method provides a full resource of ranked importance for all 'omic
492 features studied, which provides novel targets for future study.

493 There are several limitations to consider when interpreting our results. First, a common challenge
494 in unsupervised clustering endeavors, we did not achieve consensus on optimal clustering
495 solutions in our three-modal subtyping analysis. In our case, we not only examined the optimal
496 cluster number from two established methods especially suited to the SNF pipeline, but also
497 tested cluster validity by multiple resampling measures, as there is no ground truth to compare to,
498 and important information may be missed by heuristic methods alone [74],[75]. In our analysis,
499 the disagreement between optimal cluster number as elected by internal stability measures vs.
500 external cognitive and neuropathological information also demonstrates the importance of
501 transparency in the presentation of clustering analyses; in our case, both the 3- and 5-subtype
502 solutions had significant overlaps in identity, though only the fifth cluster revealed a significant
503 cognitive deficit. We again emphasize that these effects on cognition would survive correction for
504 multiple testing in a full pool of tests combining both 3- and 5-subtype solutions.

505 Second, differences in data preprocessing methods for our five 'omic data modalities may have
506 impacted downstream clustering, despite our efforts to control for technical and biological
507 confounders at both the individual feature level and at the overall sample level in models testing
508 external validity. Third, ROS/MAP is intrinsically limited by its inclusion of predominantly

509 individuals of European-Caucasian ancestry, with an overrepresentation of biologically female
510 participants [28–30]. Finally, ROS/MAP is known to be a resilient cohort of elderly individuals
511 including some members of the religious communities of Illinois. Even though we modeled study
512 as a covariate in all analyses to mitigate variability due to large lifestyle differences, results derived
513 from such a study population might not be applicable to the entire population. Future studies will
514 be required using populations with increased diversity with respect to ancestry and socio-
515 demographics. This will be the means to achieve a better understanding of the degree to which
516 our findings can be applied more broadly beyond European-Caucasians.

517

518 **List of Abbreviations**

519	AD	late-onset Alzheimer's disease
520	ADM	average distance between means
521	AMP-AD	Accelerating Medicines Partnership for Alzheimer's Disease
522	APN	average proportion of non-overlap
523	ARI	adjusted Rand index
524	CAA	cerebral amyloid angiopathy
525	DLPFC	dorsolateral prefrontal cortex
526	H3K9ac	acetylation at the 9th lysine residue of the histone H3 protein
527	MAP	Rush Memory and Aging Project
528	MCI	mild cognitive impairment
529	NMI	Normalized Mutual Information
530	PCA	Principal component analysis
531	PMI	Post mortem interval
532	RNAseq	RNA sequencing

533 ROS Religious Orders Study
534 SNF Similarity Network Fusion
535 TMT tandem mass tag
536

537 **Declarations**

538 ***Ethics approval and consent to participate***

539 For The Religious Orders Study and Rush Memory and Aging Project, all study participants
540 provided informed consent and both studies were approved by a Rush University Institutional
541 Review Board. Further, all participants signed an Anatomic Gift Act for organ donation and
542 signed a repository consent for resource sharing. For the Mayo dataset, protocols were
543 approved by the Mayo Clinic Institutional Review Board and all subjects or next of kin provided
544 informed consent.

545 ***Consent for publication***

546 Not applicable.

547 ***Availability of data and materials***

548 All multi-'omic datasets supporting the conclusions of this article are available via approved
549 access at the Synapse AMP-AD Knowledge Portal (<https://adknowledgeportal.synapse.org/>, doi:
550 10.7303/syn2580853). All analyses were performed using open-source software. No custom
551 algorithms or software were used that are central to the research or not yet described in
552 published literature. ROSMAP resources can be requested at <https://www.radc.rush.edu>.

553 ***Competing interests***

554 The authors declare no conflicts of interest. Funders did not play any role in the design,
555 analysis, or writing or this study.

556 ***Funding***

557 Funding support for DF was provided by The Koerner Family Foundation New Scientist
558 Program, The Krembil Foundation, the Canadian Institutes of Health Research, and the CAMH
559 Discovery Fund. MEC, YC, and SJT acknowledges the generous support from the CAMH
560 Discovery Fund, Krembil Foundation, Kavli Foundation, McLaughlin Foundation, Natural
561 Sciences and Engineering Research Council of Canada (RGPIN-2020-05834 and DGECR-
562 2020-00048), and Canadian Institutes of Health Research (NGN-171423 and PJT-175254), and
563 the Simons Foundation for Autism Research. ROSMAP was supported by NIH grants
564 P30AG10161, P30AG72975, R01AG15819, R01AG17917, U01AG46152 and U01AG61356.

565 ***Authors' contributions***

566 MY was responsible for data processing, statistical analysis, manuscript writing, and editing.
567 SML contributed to manuscript editing. DF was responsible for data access, ensuring data
568 quality control, study design, and manuscript writing and editing. YW, PLDJ and DAB were
569 responsible for aspects of data collection, collaborative input on study design, and manuscript
570 editing.

571 ***Acknowledgements***

572 The authors acknowledge all of the patients and their families for graciously donating brain
573 tissue. ROS/MAP is supported by Yanling Wang, Philip L De Jager and David A Bennett. Daniel
574 Felsky is supported by the Michael and Sonja Koerner New Scientist Award, the Krembil Family
575 Foundation, the Canadian Institutes of Health Research, and the CAMH Discovery Fund.
576 ROS/MAP is supported by NIH grants P30AG72971, P30AG72975, R01AG15819,
577 R01AG17917, and U01AG61356. ROS/MAP resources can be requested at
578 www.radc.rush.edu. Results published here are based on metabolomics data generated by the
579 Alzheimer's Disease Metabolomics Consortium (ADMC; ADMC members list
580 <https://sites.duke.edu/adnimetab/team/>), led by Dr. Rima Kaddurah-Daouk at Duke University,

581 using biospecimens provided by the Rush Alzheimer's Disease Center, Rush University Medical
582 Center, Chicago. Support for the biospecimen processing and data generation conducted by the
583 ADMC was provided by the following National Institute on Aging grants R01AG046171,
584 RF1AG051550, RF1AG057452, RF1AG059093, RF1AG058942, U01AG061359, and the
585 Foundation for the NIH (FNIH) grant: #DAOU16AMPA.

586

587 **References**

- 588 1. Formánek T, Csajbók Z, Wolfová K, Kučera M, Tom S, Aarsland D, et al. Trajectories of
589 depressive symptoms and associated patterns of cognitive decline. *Sci Rep.* 2020;10:20888.
- 590 2. Boyle PA, Wilson RS, Yu L, Barr AM, Honer WG, Schneider JA, et al. Much of late life
591 cognitive decline is not due to common neurodegenerative pathologies. *Ann Neurol.*
592 2013;74:478–89.
- 593 3. Nichols E, Steinmetz JD, Vollset SE, Fukutaki K, Chalek J, Abd-Allah F, et al. Estimation of
594 the global prevalence of dementia in 2019 and forecasted prevalence in 2050: an analysis for
595 the Global Burden of Disease Study 2019. *Lancet Public Health.* 2022;7:e105–25.
- 596 4. Breijyeh Z, Karaman R. Comprehensive Review on Alzheimer's Disease: Causes and
597 Treatment. *Molecules.* 2020;25:5789.
- 598 5. Bennett DA, Schneider JA, Arvanitakis Z, Kelly JF, Aggarwal NT, Shah RC, et al.
599 Neuropathology of older persons without cognitive impairment from two community-based
600 studies. *Neurology.* 2006;66:1837–44.
- 601 6. Jiang Y-Z, Liu Y, Xiao Y, Hu X, Jiang L, Zuo W-J, et al. Molecular subtyping and genomic
602 profiling expand precision medicine in refractory metastatic triple-negative breast cancer: the
603 FUTURE trial. *Cell Res.* 2021;31:178–86.
- 604 7. Zhao L, Lee VHF, Ng MK, Yan H, Bijlsma MF. Molecular subtyping of cancer: current status
605 and moving toward clinical applications. *Brief Bioinform.* 2019;20:572–84.
- 606 8. Neff RA, Wang M, Vatansever S, Guo L, Ming C, Wang Q, et al. Molecular subtyping of
607 Alzheimer's disease using RNA sequencing data reveals novel mechanisms and targets. *Sci
608 Adv.* 2021;7:eabb5398.
- 609 9. Zheng C, Xu R. Molecular subtyping of Alzheimer's disease with consensus non-negative
610 matrix factorization. *PLoS One.* 2021;16:e0250278.

611 10. Olah M, Menon V, Habib N, Taga MF, Ma Y, Yung CJ, et al. Single cell RNA sequencing of
612 human microglia uncovers a subset associated with Alzheimer's disease. *Nat Commun.*
613 2020;11:6129.

614 11. Ma M, Liao Y, Huang X, Zou C, Chen L, Liang L, et al. Identification of Alzheimer's Disease
615 Molecular Subtypes Based on Parallel Large-Scale Sequencing. *Front Aging Neurosci.*
616 2022;14:770136.

617 12. Emon MA, Heinson A, Wu P, Domingo-Fernández D, Sood M, Vrooman H, et al. Clustering
618 of Alzheimer's and Parkinson's disease based on genetic burden of shared molecular
619 mechanisms. *Sci Rep.* 2020;10:19097.

620 13. Picard M, Scott-Boyer M-P, Bodein A, Périn O, Droit A. Integration strategies of multi-omics
621 data for machine learning analysis. *Comput Struct Biotechnol J.* 2021;19:3735–46.

622 14. Misra BB, Langefeld C, Olivier M, Cox LA. Integrated omics: tools, advances and future
623 approaches. *J Mol Endocrinol.* 2019;62:R21–45.

624 15. Klein H-U, McCabe C, Gjoneska E, Sullivan SE, Kaskow BJ, Tang A, et al. Epigenome-wide
625 study uncovers large-scale changes in histone acetylation driven by tau pathology in aging and
626 Alzheimer's human brains. *Nat Neurosci.* 2019;22:37–46.

627 16. Huo Z, Yu L, Yang J, Zhu Y, Bennett DA, Zhao J. Brain and blood metabolome for
628 Alzheimer's dementia: findings from a targeted metabolomics analysis. *Neurobiol Aging.*
629 2020;86:123–33.

630 17. Wang G, Zhou Y, Huang F-J, Tang H-D, Xu X-H, Liu J-J, et al. Plasma Metabolite Profiles of
631 Alzheimer's Disease and Mild Cognitive Impairment. *J Proteome Res.* 2014;13:2649–58.

632 18. Toledo JB, Arnold M, Kastenmüller G, Chang R, Baillie RA, Han X, et al. Metabolic network
633 failures in Alzheimer's disease: A biochemical road map. *Alzheimers Dement J Alzheimers*
634 *Assoc.* 2017;13:965–84.

635 19. Arnold M, Nho K, Kueider-Paisley A, Massaro T, Huynh K, Brauner B, et al. Sex and APOE
636 ε4 genotype modify the Alzheimer's disease serum metabolome. *Nat Commun.* 2020;11:1148.

637 20. St John-Williams L, Blach C, Toledo JB, Rotroff DM, Kim S, Klavins K, et al. Targeted
638 metabolomics and medication classification data from participants in the ADNI1 cohort. *Sci*
639 *Data.* 2017;4:170140.

640 21. Johnson ECB, Carter EK, Dammer EB, Duong DM, Gerasimov ES, Liu Y, et al. Large-scale
641 deep multi-layer analysis of Alzheimer's disease brain reveals strong proteomic disease-related
642 changes not observed at the RNA level. *Nat Neurosci.* 2022;25:213–25.

643 22. Badhwar A, McFall GP, Sapkota S, Black SE, Chertkow H, Duchesne S, et al. A multiomics
644 approach to heterogeneity in Alzheimer's disease: focused review and roadmap. *Brain.*
645 2020;143:1315–31.

646 23. Singh A, Shannon CP, Gautier B, Rohart F, Vacher M, Tebbutt SJ, et al. DIABLO: an
647 integrative approach for identifying key molecular drivers from multi-omics assays. Birol I, editor.
648 *Bioinformatics.* 2019;35:3055–62.

649 24. Ma Y, Klein H, De Jager PL. Considerations for integrative multi - omic approaches to
650 explore Alzheimer's disease mechanisms. *Brain Pathol.* 2020;bpa.12878.

651 25. Rappoport N, Shamir R. Multi-omic and multi-view clustering algorithms: review and cancer
652 benchmark. *Nucleic Acids Res.* 2018;46:10546–62.

653 26. Chauvel C, Novoloaca A, Veyre P, Reynier F, Becker J. Evaluation of integrative clustering
654 methods for the analysis of multi-omics data. *Brief Bioinform.* 2020;21:541–52.

655 27. Wang B, Mezlini AM, Demir F, Fiume M, Tu Z, Brudno M, et al. Similarity network fusion for
656 aggregating data types on a genomic scale. *Nat Methods.* 2014;11:333–7.

657 28. Bennett DA, Buchman AS, Boyle PA, Barnes LL, Wilson RS, Schneider JA. Religious
658 Orders Study and Rush Memory and Aging Project. *J Alzheimers Dis JAD.* 2018;64:S161–89.

659 29. De Jager PL, Ma Y, McCabe C, Xu J, Vardarajan BN, Felsky D, et al. A multi-omic atlas of
660 the human frontal cortex for aging and Alzheimer's disease research. *Sci Data.* 2018;5:180142.

661 30. Bennett DA, Schneider JA, Buchman AS, Barnes LL, Boyle PA, Wilson RS. Overview and
662 findings from the rush Memory and Aging Project. *Curr Alzheimer Res.* 2012;9:646–63.

663 31. Felsky D, Klein H-U, Menon V, Ma Y, Wang Y, Milic M, et al. Human peripheral monocytes
664 capture elements of the state of microglial activation in the brain [Internet]. In Review; 2022 Jan.
665 Available from: <https://www.researchsquare.com/article/rs-1226021/v1>

666 32. Rybnicek J, Chen Y, Milic M, McLaurin J, De Jager PL, Schneider JA, et al. Common
667 genetic variants in *CHRNA5* alter β -amyloid neuropathology and highlight chandelier cells in
668 human aging and Alzheimer's disease [Internet]. *Neuroscience*; 2022 May. Available from:
669 <http://biorxiv.org/lookup/doi/10.1101/2022.05.03.490491>

670 33. De Jager PL, Srivastava G, Lunnon K, Burgess J, Schalkwyk LC, Yu L, et al. Alzheimer's
671 disease: early alterations in brain DNA methylation at ANK1, BIN1, RHBD2 and other loci. *Nat*
672 *Neurosci.* 2014;17:1156–63.

673 34. Wei R, Wang J, Su M, Jia E, Chen S, Chen T, et al. Missing Value Imputation Approach for
674 Mass Spectrometry-based Metabolomics Data. *Sci Rep.* 2018;8:663.

675 35. Wingo TS, Duong DM, Zhou M, Dammer EB, Wu H, Cutler DJ, et al. Integrating Next-
676 Generation Genomic Sequencing and Mass Spectrometry To Estimate Allele-Specific Protein
677 Abundance in Human Brain. *J Proteome Res.* 2017;16:3336–47.

678 36. Mertins P, Tang LC, Krug K, Clark DJ, Gritsenko MA, Chen L, et al. Reproducible workflow
679 for multiplexed deep-scale proteome and phosphoproteome analysis of tumor tissues by liquid
680 chromatography–mass spectrometry. *Nat Protoc.* 2018;13:1632–61.

681 37. Kokla M, Virtanen J, Kolehmainen M, Paananen J, Hanhineva K. Random forest-based
682 imputation outperforms other methods for imputing LC-MS metabolomics data: a comparative
683 study. *BMC Bioinformatics.* 2019;20:492.

684 38. Mostafavi S, Gaiteri C, Sullivan SE, White CC, Tasaki S, Xu J, et al. A molecular network of
685 the aging human brain provides insights into the pathology and cognitive decline of Alzheimer's
686 disease. *Nat Neurosci*. 2018;21:811–9.

687 39. Consensus Recommendations for the Postmortem Diagnosis of Alzheimer's Disease.
688 *Neurobiol Aging*. 1997;18:S1–2.

689 40. Wilson RS, Boyle PA, Yu L, Barnes LL, Sytsma J, Buchman AS, et al. Temporal course and
690 pathologic basis of unawareness of memory loss in dementia. *Neurology*. 2015;85:984–91.

691 41. De Jager PL, Shulman JM, Chibnik LB, Keenan BT, Raj T, Wilson RS, et al. A genome-wide
692 scan for common variants affecting the rate of age-related cognitive decline. *Neurobiol Aging*.
693 2012;33:1017.e1-1017.e15.

694 42. Bocancea DI, van Loenhoud AC, Groot C, Barkhof F, van der Flier WM, Ossenkoppele R.
695 Measuring Resilience and Resistance in Aging and Alzheimer Disease Using Residual
696 Methods: A Systematic Review and Meta-analysis. *Neurology*. 2021;97:474–88.

697 43. Consens ME, Chen Y, Menon V, Wang Y, Schneider JA, De Jager PL, et al. Bulk and
698 Single-Nucleus Transcriptomics Highlight Intra-Telencephalic and Somatostatin Neurons in
699 Alzheimer's Disease. *Front Mol Neurosci*. 2022;15:903175.

700 44. Stefanik L, Erdman L, Ameis SH, Foussias G, Mulsant BH, Behdinan T, et al. Brain-
701 Behavior Participant Similarity Networks Among Youth and Emerging Adults with Schizophrenia
702 Spectrum, Autism Spectrum, or Bipolar Disorder and Matched Controls.
703 *Neuropsychopharmacology*. 2018;43:1180–8.

704 45. Park S, Zhao H. Spectral clustering based on learning similarity matrix. *Bioinforma Oxf Engl*.
705 2018;34:2069–76.

706 46. Huang J, Nie F, Huang H. Spectral Rotation versus K-Means in Spectral Clustering. *Proc
707 AAAI Conf Artif Intell*. 2013;27:431–7.

708 47. Estevez PA, Tesmer M, Perez CA, Zurada JM. Normalized Mutual Information Feature
709 Selection. *IEEE Trans Neural Netw*. 2009;20:189–201.

710 48. Handl J, Knowles J, Kell DB. Computational cluster validation in post-genomic data analysis.
711 *Bioinformatics*. 2005;21:3201–12.

712 49. Brock G, Pihur V, Datta S, Datta S. **cIViVal** : An *R* Package for Cluster Validation. *J Stat
713 Softw* [Internet]. 2008 [cited 2022 Sep 17];25. Available from: <http://www.jstatsoft.org/v25/i04/>

714 50. Department of Bioinformatics and Biostatistics, University of Louisville, Louisville, Kentucky,
715 40202, USA, Sekula M, Datta S, Department of Biostatistics, University of Florida, Gainesville,
716 Florida, 32611, USA, Datta S, Department of Biostatistics, University of Florida, Gainesville,
717 Florida, 32611, USA. *optCluster*: An *R* Package for Determining the Optimal Clustering
718 Algorithm. *Bioinformation*. 2017;13:101–3.

719 51. Yan L, Yang M, Guo H, Yang L, Wu J, Li R, et al. Single-cell RNA-Seq profiling of human
720 preimplantation embryos and embryonic stem cells. *Nat Struct Mol Biol*. 2013;20:1131–9.

721 52. Jacobs GR, Voineskos AN, Hawco C, Stefanik L, Forde NJ, Dickie EW, et al. Integration of
722 brain and behavior measures for identification of data-driven groups cutting across children with
723 ASD, ADHD, or OCD. *Neuropsychopharmacology*. 2021;46:643–53.

724 53. Chacón JE, Rastrojo AI. Minimum adjusted Rand index for two clusterings of a given size.
725 *Adv Data Anal Classif* [Internet]. 2022 [cited 2022 Oct 6]; Available from:
726 <https://link.springer.com/10.1007/s11634-022-00491-w>

727 54. Cohen JE. The Distribution of the Chi-Squared Statistic under Clustered Sampling from
728 Contingency Tables. *J Am Stat Assoc*. 1976;71:665–70.

729 55. Kent WJ, Sugnet CW, Furey TS, Roskin KM, Pringle TH, Zahler AM, et al. The Human
730 Genome Browser at UCSC. *Genome Res*. 2002;12:996–1006.

731 56. Alashwal H, El Halaby M, Crouse JJ, Abdalla A, Moustafa AA. The Application of
732 Unsupervised Clustering Methods to Alzheimer’s Disease. *Front Comput Neurosci*. 2019;13:31.

733 57. Hamamoto R, Komatsu M, Takasawa K, Asada K, Kaneko S. Epigenetics Analysis and
734 Integrated Analysis of Multiomics Data, Including Epigenetic Data, Using Artificial Intelligence in
735 the Era of Precision Medicine. *Biomolecules*. 2019;10:62.

736 58. Elliott GO, Johnson IT, Scarll J, Dainty J, Williams EA, Garg D, et al. Quantitative profiling of
737 CpG island methylation in human stool for colorectal cancer detection. *Int J Colorectal Dis*.
738 2013;28:35–42.

739 59. Leygo C, Williams M, Jin HC, Chan MWY, Chu WK, Grusch M, et al. DNA Methylation as a
740 Noninvasive Epigenetic Biomarker for the Detection of Cancer. *Dis Markers*. 2017;2017:1–13.

741 60. Scheubert L, Luštrek M, Schmidt R, Repsilber D, Fuellen G. Tissue-based Alzheimer gene
742 expression markers—comparison of multiple machine learning approaches and investigation of
743 redundancy in small biomarker sets. *BMC Bioinformatics*. 2012;13:266.

744 61. Li QS, De Muynck L. Differentially expressed genes in Alzheimer’s disease highlighting the
745 roles of microglia genes including OLR1 and astrocyte gene CDK2AP1. *Brain Behav Immun -*
746 *Health*. 2021;13:100227.

747 62. Liu D, Dai S-X, He K, Li G-H, Liu J, Liu LG, et al. Identification of hub ubiquitin ligase genes
748 affecting Alzheimer’s disease by analyzing transcriptome data from multiple brain regions. *Sci
749 Prog*. 2021;104:003685042110011.

750 63. Vastrand B, Vastrand C. Bioinformatics analyses of significant genes, related pathways and
751 candidate prognostic biomarkers in Alzheimer’s disease [Internet]. *Bioinformatics*; 2021 May.
752 Available from: <http://biorxiv.org/lookup/doi/10.1101/2021.05.06.442918>

753 64. Kim DY, Ingano LAM, Kovacs DM. Nectin-1 α , an Immunoglobulin-like Receptor Involved in
754 the Formation of Synapses, Is a Substrate for Presenilin/ γ -Secretase-like Cleavage. *J Biol
755 Chem*. 2002;277:49976–81.

756 65. De Paepe B, Merckx C, Jarošová J, Cannizzaro M, De Bleeker JL. Myo-Inositol
757 Transporter SLC5A3 Associates with Degenerative Changes and Inflammation in Sporadic
758 Inclusion Body Myositis. *Biomolecules*. 2020;10:521.

759 66. Braithwaite SP, Stock JB, Lombroso PJ, Nairn AC. Protein Phosphatases and Alzheimer's
760 Disease. *Prog Mol Biol Transl Sci* [Internet]. Elsevier; 2012 [cited 2022 Oct 14]. p. 343–79.
761 Available from: <https://linkinghub.elsevier.com/retrieve/pii/B9780123964564000122>

762 67. Kaut O, Schmitt I, Wüllner U. Genome-scale methylation analysis of Parkinson's disease
763 patients' brains reveals DNA hypomethylation and increased mRNA expression of cytochrome
764 P450 2E1. *neurogenetics*. 2012;13:87–91.

765 68. Aarsland D, Creese B, Politis M, Chaudhuri KR, ffytche DH, Weintraub D, et al. Cognitive
766 decline in Parkinson disease. *Nat Rev Neurol*. 2017;13:217–31.

767 69. Lokireddy S, Kukushkin NV, Goldberg AL. cAMP-induced phosphorylation of 26S
768 proteasomes on Rpn6/PSMD11 enhances their activity and the degradation of misfolded
769 proteins. *Proc Natl Acad Sci* [Internet]. 2015 [cited 2022 Oct 9];112. Available from:
770 <https://pnas.org/doi/full/10.1073/pnas.1522332112>

771 70. Giri M, Shah A, Upreti B, Rai JC. Unraveling the genes implicated in Alzheimer's disease.
772 *Biomed Rep*. 2017;7:105–14.

773 71. Yuan S-X, Li H-T, Gu Y, Sun X. Brain-Specific Gene Expression and Quantitative Traits
774 Association Analysis for Mild Cognitive Impairment. *Biomedicines*. 2021;9:658.

775 72. Clough RL, Dermentzaki G, Stefanis L. Functional dissection of the α -synuclein promoter:
776 transcriptional regulation by ZSCAN21 and ZNF219. *J Neurochem*. 2009;110:1479–90.

777 73. Barrachina M, Ferrer I. DNA Methylation of Alzheimer Disease and Tauopathy-Related
778 Genes in Postmortem Brain. *J Neuropathol Exp Neurol*. 2009;68:880–91.

779 74. Fang Y, Wang J. Selection of the number of clusters via the bootstrap method. *Comput Stat
780 Data Anal*. 2012;56:468–77.

781 75. Horne E, Tibble H, Sheikh A, Tsanas A. Challenges of Clustering Multimodal Clinical Data:
782 Review of Applications in Asthma Subtyping. *JMIR Med Inform*. 2020;8:e16452.

783

784

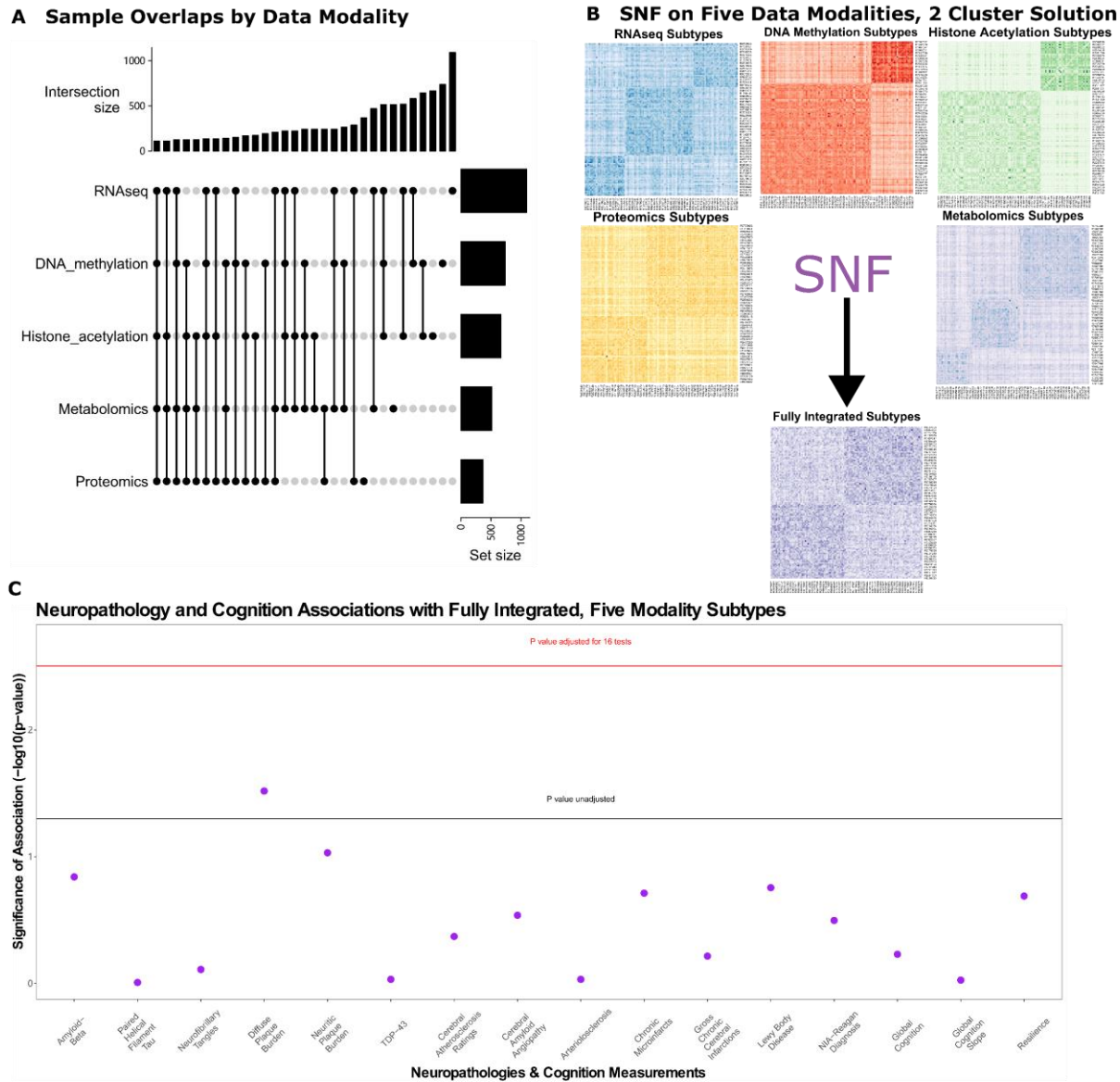
785 **Tables**

786 **Table 1. Table summarizing demographic data and the availability of multi-'omic data modalities**
787 **stratified by NIA-Reagan diagnosis criteria in ROS/MAP**

Total n = 1,314 individuals with post-mortem measurement			
	Non-AD (n=475)	AD (n=838)	Total
Age at Baseline	79.62 (7.25)	81.46 (6.62)	80.81 (6.91)
Age of Death	87.55 (7.12)	90.27 (6.11)	89.28 (6.62)
Biological Sex (0: female, 1: male)	38.95%	29.24%	32.75%
Post Mortem Interval	8.32 (6.31)	8.32 (5.92)	8.32 (6.06)
APOE E4 (0: without E4, 1: with E4)	13.05%	32.36%	25.74%
Year of Education	16.34 (3.55)	16.10 (3.55)	16.19 (3.55)
Proportion of participants with non-missing data for each data type			
RNA-Seq	84.84%	84.22%	83.17%
DNA Methylation	61.26%	53.46%	56.28%
Histone Acetylation	53.68%	49.28%	50.88%
Metabolomics	36.00%	40.93%	39.15%
Proteomics	31.79%	25.89%	28.03%

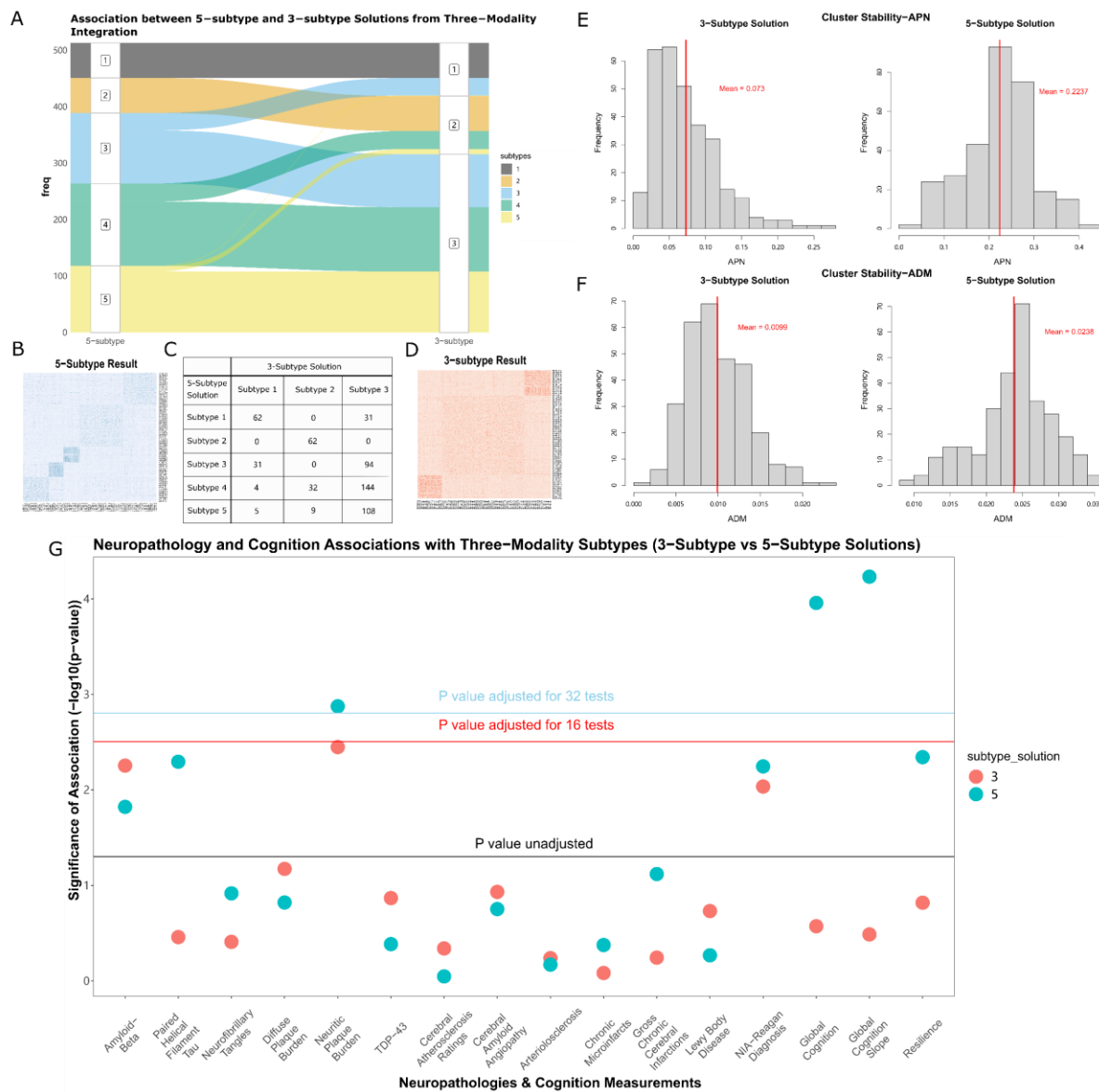
788 All participants in the sample space have at least one 'omic data modality and phenotype data available,
789 mean and standard deviation is recorded.

790 **Figures**



792 **Figure 1. Molecular subtypes derived from 5 multi-'omic data modalities via SNF.** A) Overlapping
793 sample sizes across all combinations between five data modalities were examined using upset plot. B)
794 Unimodal subtypes were identified from affinity matrices using spectral clustering accordingly from 111
795 overlapping samples (RNAseq: three subtypes, DNA methylation: two subtypes, histone acetylation: two
796 subtypes, proteomics: two subtypes, metabolomics: three subtypes). Fully integrated subtypes were
797 illustrated in the affinity matrix as well. C) Associations of fully integrated subtype memberships and 16 age-

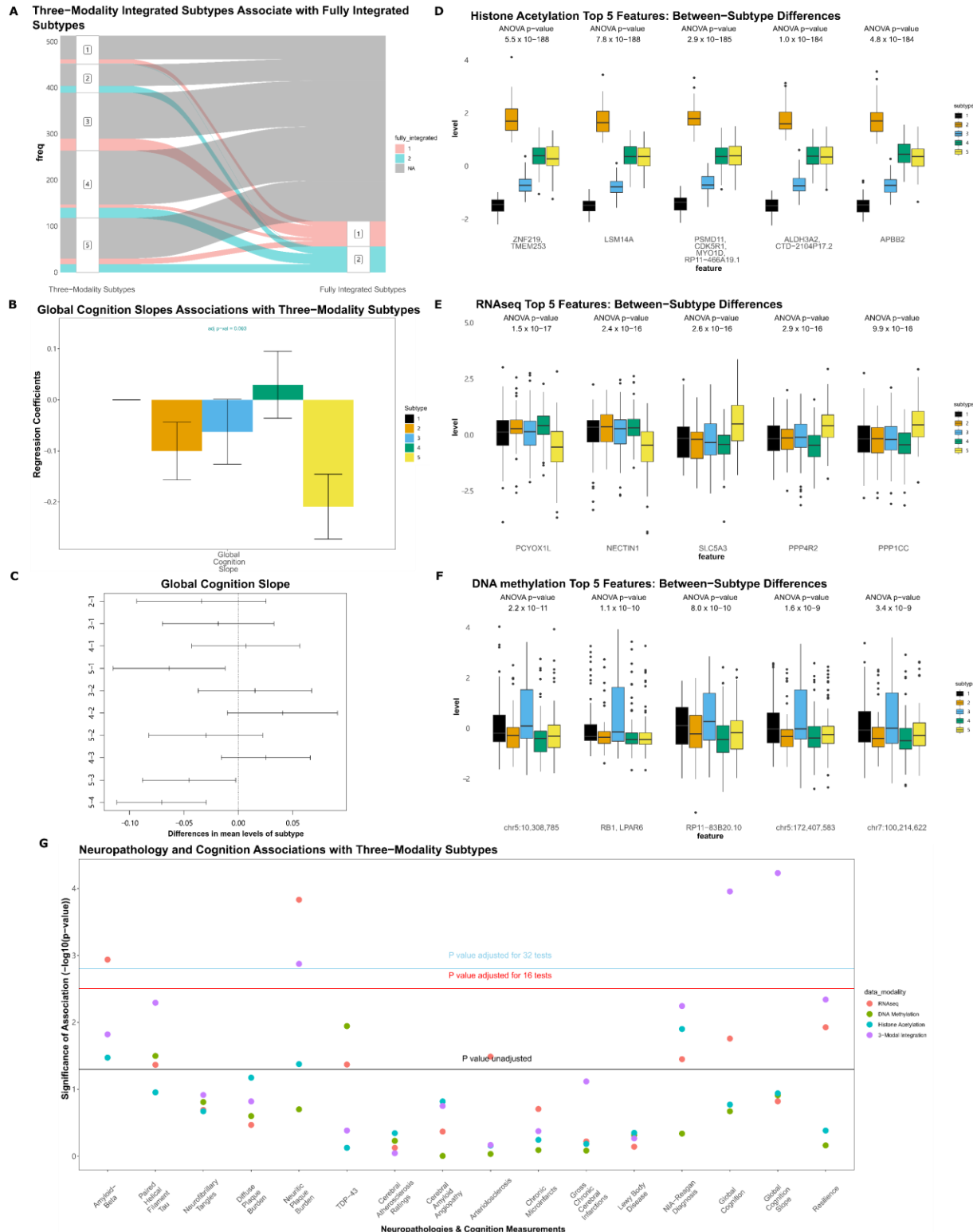
798 related neuropathologies and cognitive measurements were examined by omnibus F-tests for linear
799 regression models. Y-axis shows significance of association (-log₁₀ transformed raw p-values). The black
800 horizontal line illustrates an unadjusted *p*-value threshold at 0.05, whereas the purple horizontal line
801 demonstrates Bonferroni-adjusted *p*-value thresholds for 16 tests ($p_{\text{raw}}=3.1 \times 10^{-3}$).



802

803 **Figure 2. Two subtyping solutions derived from histone acetylation, DNA methylation and RNAseq**
 804 **were tested against each other both internally and externally.** A) 3-subtype solution and 5-subtype
 805 solution derived from 3-modal integrated networks were associated with each other. B-D) Subtypes were
 806 identified from affinity matrices using spectral clustering, and overlapped with each other E) Histograms for
 807 the distribution of ADM generated from 300 random sub-samples for both 3-subtype and 5-subtype
 808 solutions. F) Histograms for the distribution of APN generated from 300 random sub-samples for both 3-
 809 subtype and 5-subtype solutions. G) Associations of 3-modal integrated memberships and 16 age-related
 810 neurobiological traits were examined by omnibus F-tests for linear regression models. Y-axis shows

811 significance of association (-log₁₀ transformed raw p-values). The black horizontal line illustrates an
812 unadjusted *p*-value threshold at 0.05, whereas the red and blue horizontal lines demonstrate Bonferroni-
813 adjusted *p*-value thresholds for 16 and 32 tests ($p_{\text{raw}}=3.1 \times 10^{-3}$ and $p_{\text{raw}}=1.6 \times 10^{-3}$), respectively. Two
814 subtyping solutions for molecular subtyping were differentiated by color.

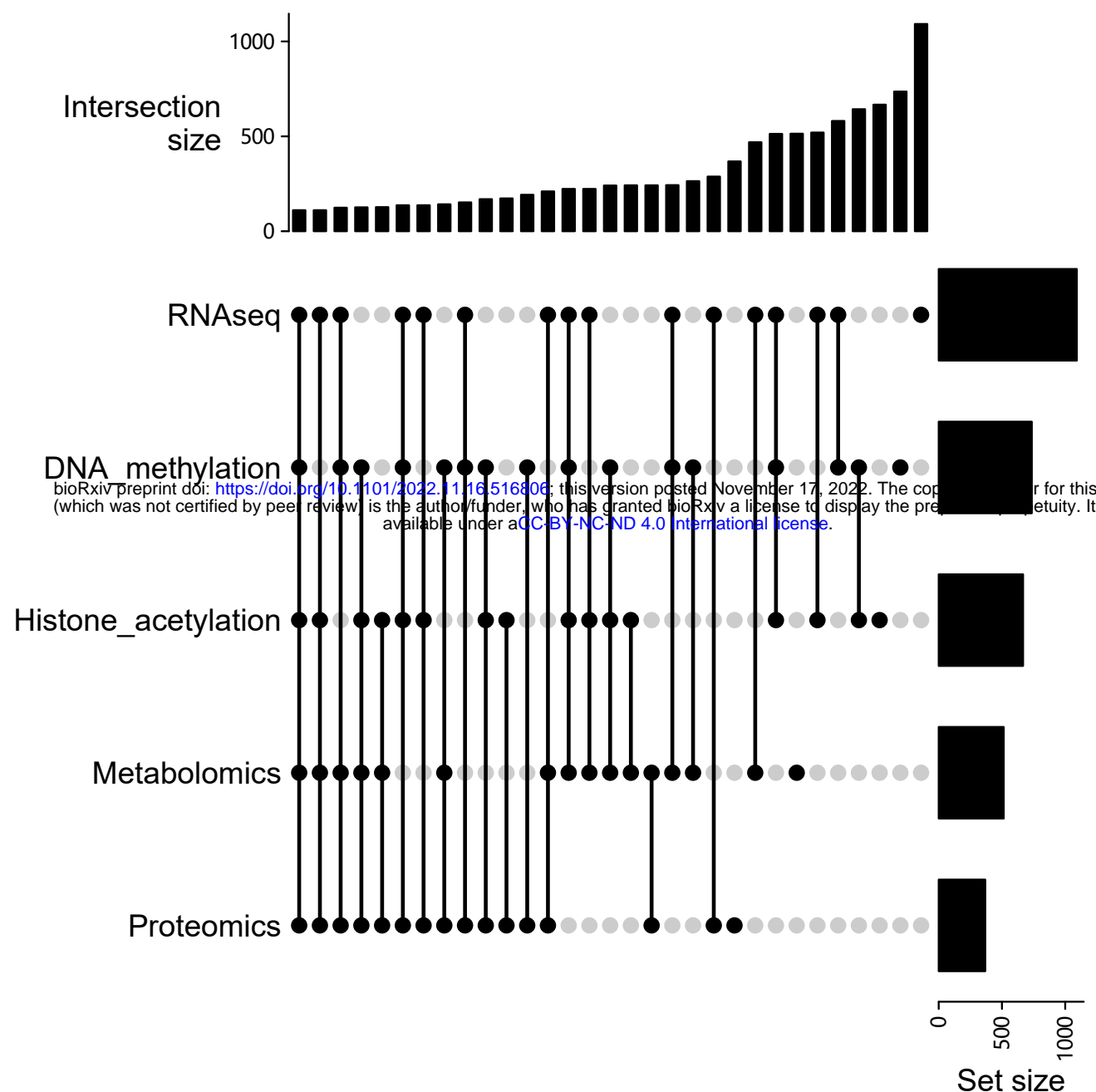


815

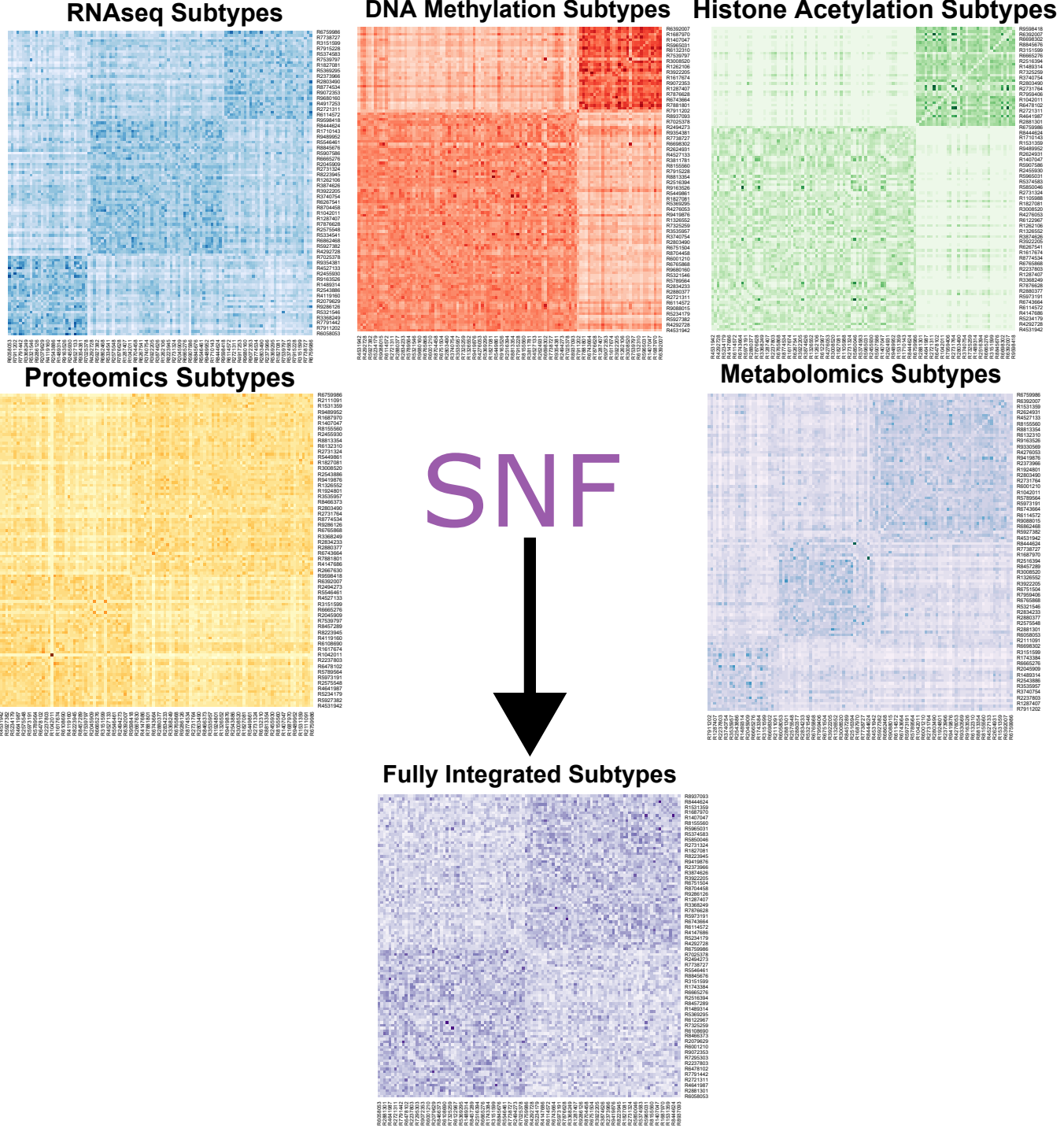
816 **Figure 3. Molecular subtypes derived from histone acetylation, DNA methylation and RNAseq were**
 817 **tested against age-related neuropathologies and cognitive measurements. A) Subtypes derived from**

818 three-modal integrated networks were associated with the fully integrated subtypes. B) Consensus
819 associations of three-modal integrated subtypes and rate of cognitive decline. Y-axis shows standardized
820 beta coefficients estimated from linear regression, where subtype 1 was used as the baseline category
821 (error bars show standard deviation from standardized linear regression models). C) Difference in mean
822 value of rate of cognitive decline between subtypes by Tukey's HSD. D-F) Boxplots showing the z-
823 normalized values of the top 5 features contributing to the three-modal fused network from each input data
824 modality. G) Associations of 3-modal integrated and unimodal subtype memberships with
825 neuropathological and cognitive traits were examined by omnibus F-tests for linear regression models. Y-
826 axis shows significance of association (-log₁₀ transformed raw p-values). The black horizontal line illustrates
827 an unadjusted p-value threshold at 0.05, whereas the red and blue horizontal lines demonstrate Bonferroni-
828 adjusted p-value thresholds for 16 and 32 tests ($p_{\text{raw}}=3.1 \times 10^{-3}$ and $p_{\text{raw}}=1.6 \times 10^{-3}$), respectively. Data
829 modalities used for molecular subtyping were differentiated by color.

A Sample Overlaps by Data Modality

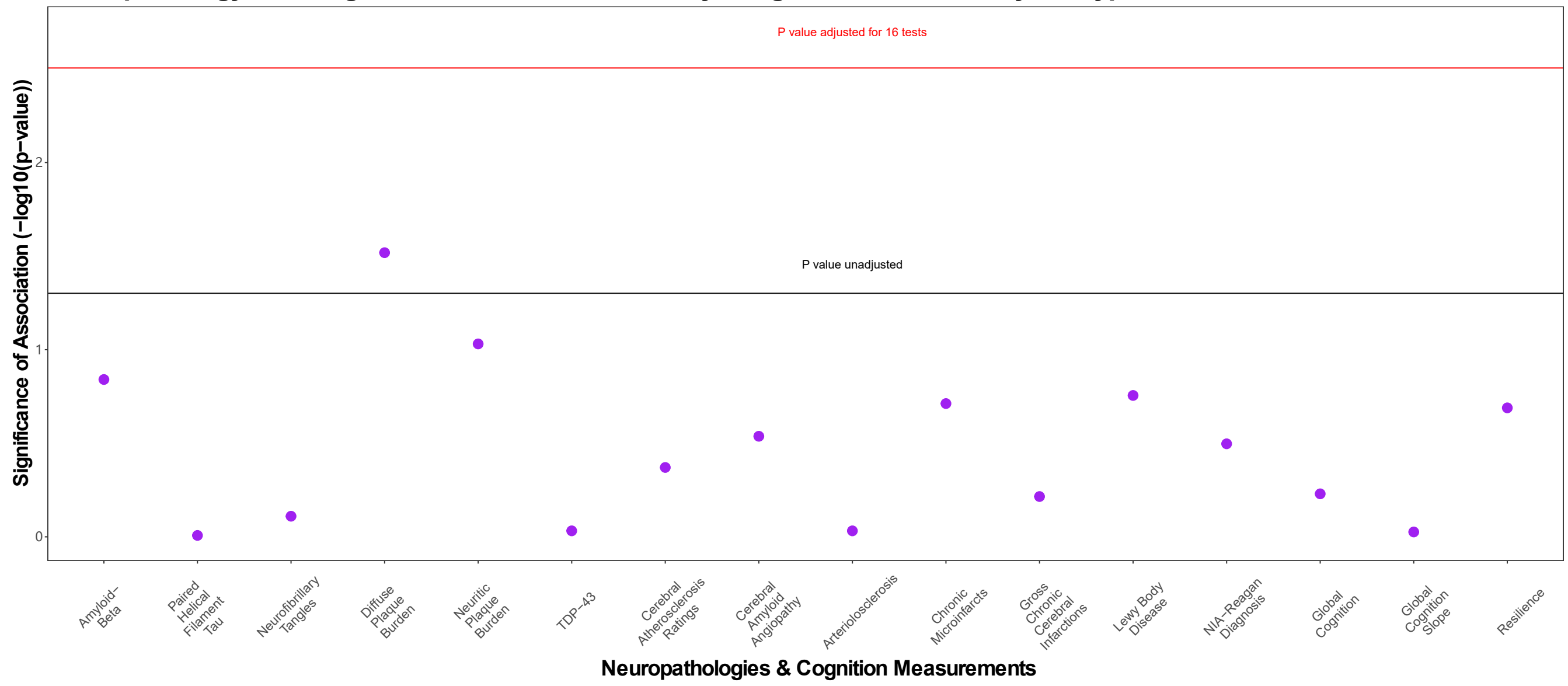


B SNF on Five Data Modalities, 2 Cluster Solution

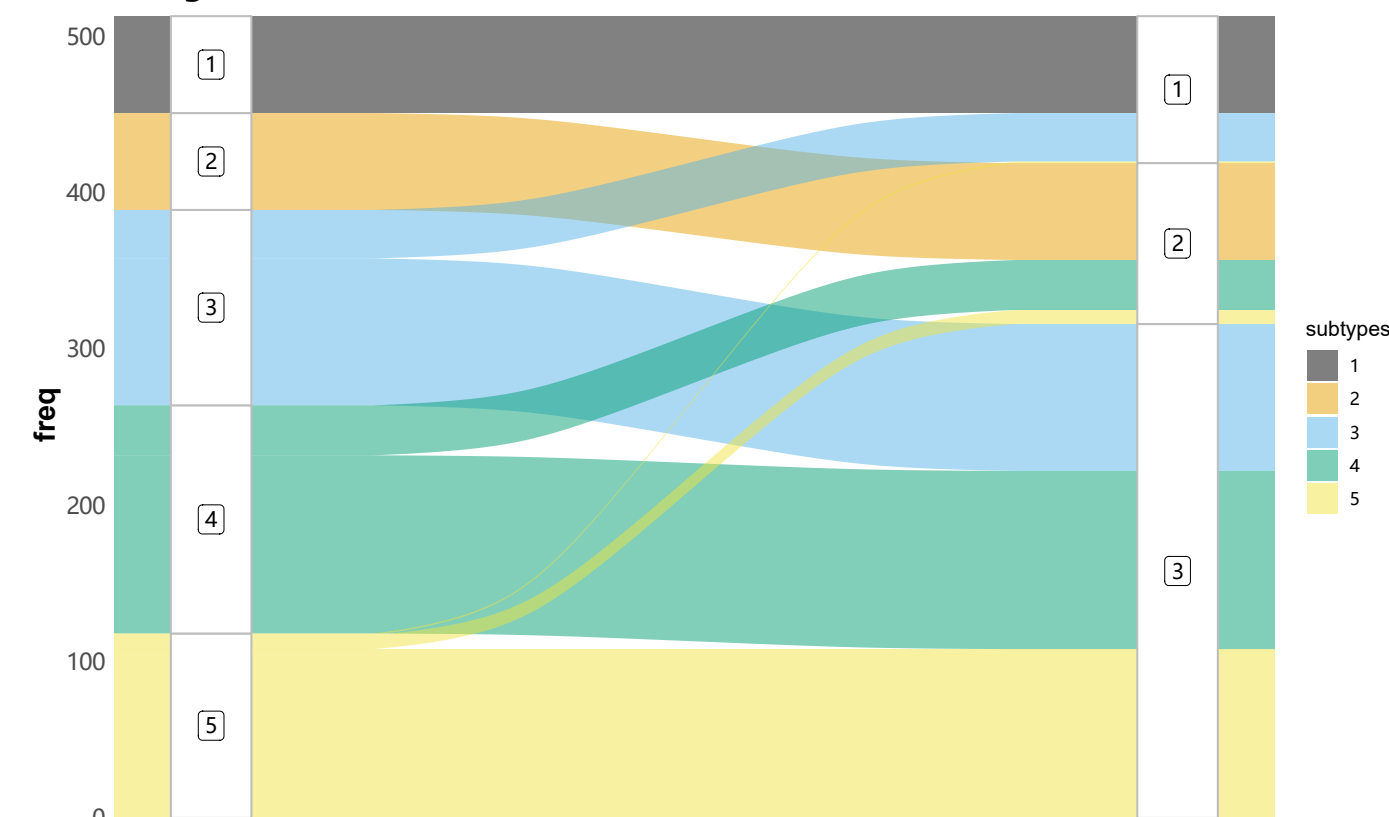


C

Neuropathology and Cognition Associations with Fully Integrated, Five Modality Subtypes

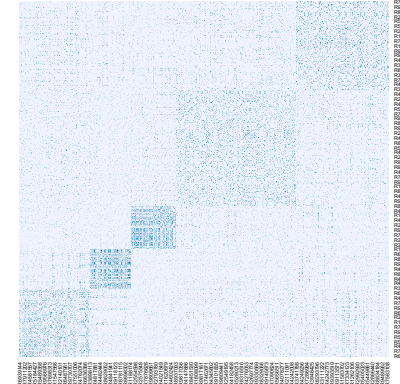


A Association between 5-subtype and 3-subtype Solutions from Three-Modality Integration



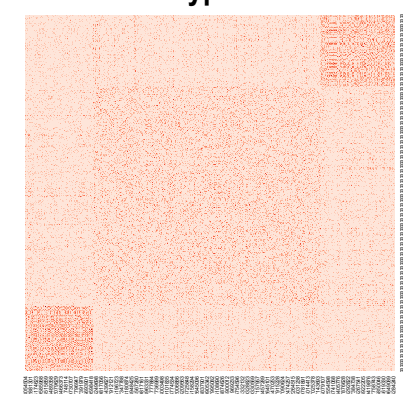
bioRxiv preprint doi: <https://doi.org/10.1101/2022.11.16.516806>; this version posted November 17, 2022. The copyright holder for this preprint (which was not certified by peer review) is the author/funder, who has granted bioRxiv a license to display the preprint in perpetuity. It is made available under aCC-BY-NC-ND 4.0 International license.

5-Subtype Result



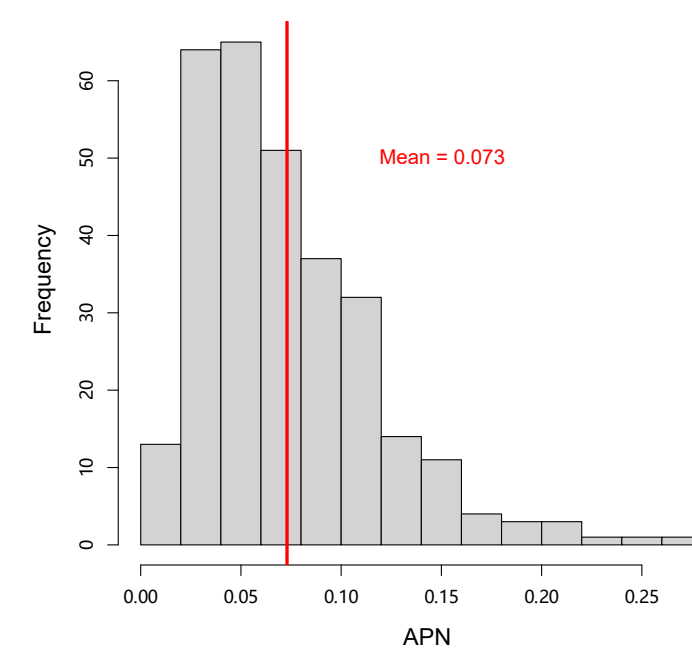
5-Subtype Solution	3-Subtype Solution		
	Subtype 1	Subtype 2	Subtype 3
Subtype 1	62	0	31
Subtype 2	0	62	0
Subtype 3	31	0	94
Subtype 4	4	32	144
Subtype 5	5	9	108

3-Subtype Result

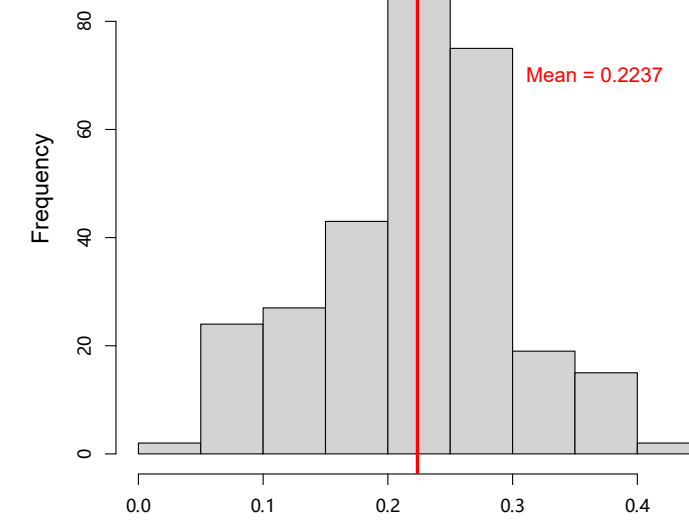


E

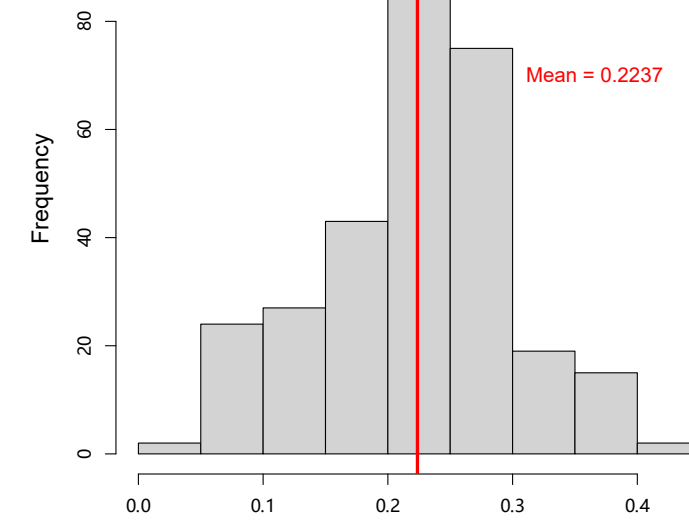
3-Subtype Solution



Cluster Stability-APN

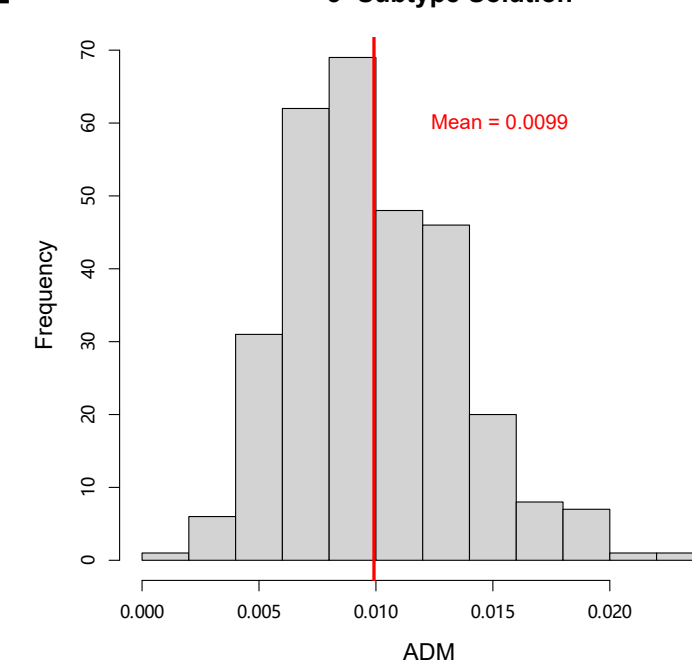


5-Subtype Solution

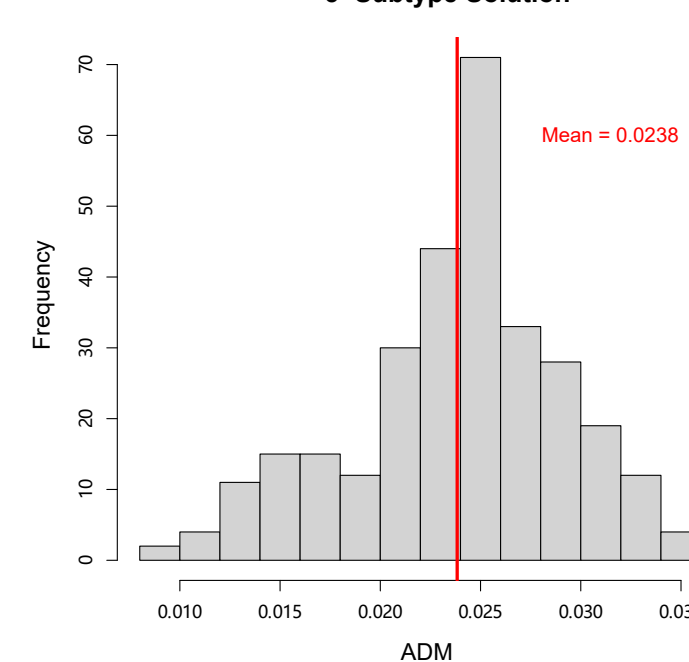


F

3-Subtype Solution



Cluster Stability-ADM



G Neuropathology and Cognition Associations with Three-Modality Subtypes (3-Subtype vs 5-Subtype Solutions)

